Associative Detachment of O^- with CO, H_2, and O_2†

J. L. Mauer* and G. J. Schulz
Mason Laboratory, Yale University, New Haven, Connecticut 06520
(Received 31 July 1972)

The associative detachment reactions of O^- with CO, H_2, and O_2 are studied experimentally using an ion beam (0–10 eV) impinging on a gas-filled chamber. The resultant electrons are energy analyzed using retarding potentials. At low ion energy, cross sections for total electron detachment for the reactions of O^- with CO and H_2 vary as the inverse of the relative velocity. At higher energies, the cross sections show a broad peak. We interpret this shape in terms of the potential-energy curves of the compound states. The energy distributions for the electrons resulting from the reactions of O^- with CO and H_2 exhibit peaks at low energy corresponding to the excitation of high vibrational and rotational states of the resultant triatomic molecules (CO_2, H_2O). Progressions observed in these distributions have spacings corresponding to the preferential excitation of the bending modes of the triatomic molecules. The cross section for total electron detachment for the reaction of O^- with O_2 exhibits a threshold near 0.7 eV and rises linearly at higher energy.

I. INTRODUCTION

Associative detachment is an ion-molecule (atom) reaction of the form

$$A^- + B \rightarrow AB + e + \Delta E ,$$

where A^- is a negative ion, B is an atom or molecule, AB is the resultant molecule which may be in an excited state, and e is the free electron. The reaction is exothermic if the dissociation energy of the molecule AB is greater than the electron affinity of A. In some associative detachment reactions, this difference can be relatively large (~3 eV) and might yield fast electrons; alternately, the molecule AB could absorb the excess energy in vibrational, rotational, or electronic excitation, and the reaction thus could lead to the production of slow electrons.

Associative detachment reactions are important in the upper atmosphere where they increase the electron density at night, when photodetachment and photoionization are less significant.[1] Indeed, such associative detachment reactions compete with charge transfer in the destruction of O^- and O_2^-.[2,3] The associative detachment reaction of H^- with H appears to be competitive with photodetachment in some regions of the solar photosphere,[1,4] although it does not determine the balance between H and H_2. The resultant H_2 is expected to be vibrationally excited.[5]

Bates and Massey[6] outlined a theory of electron detachment based on a model of curve crossings. The model required a zero-order curve crossing of the potential-energy curves of the negative-ion complex AB^- and the molecule AB. The theory contained, as parameters, the internuclear separation of the crossing point and the time for electron detachment after the crossing is passed. This lifetime is a function of the potential curves. Later, Browne and Dalgarno[7] applied this theory, appropriately extended, to the reaction of H^- with H using the potential-energy curves of Bardsley, Herzenberg, and Mandl,[8] as well as those of Chen and Peacher.[9]

The theoretical model later developed for associative detachment is closely related to the model for its inverse, dissociative attachment. Dissociative attachment is more easily studied and, therefore, extensively investigated. It is a two-stage process, the first stage being the electron capture into a compound state AB^-*. In the second stage, the nuclei separate into an ion and a neutral fragment. During this separation, the compound state can decay by the emission of an electron into the ground electronic state, possibly with vibrational excitation. Associative detachment occurs through the same compound state,[10] and it is the description of the compound state that is common to both models. The initial impetus for this work was the desire to probe experimentally the compound states from large internuclear separations by using associative detachment.

Two theories for associative detachment have been developed. Chen and Peacher[9] have derived the cross section for the associative detachment reaction of H^- with H by using experimental information[11,12] of the inverse reaction (dissociative attachment) to determine theoretical parameters. Herzenberg[13] has developed a theory of electron detachment proceeding from a formulation originally developed for dissociative attachment. He has also estimated the maximum cross section as a function of negative-ion energy. This is particularly appropriate because several of the systems considered here have short lifetimes which would suggest that they might reach this maximum.

Previous experimental work on associative detachment has been limited to low negative-ion en-

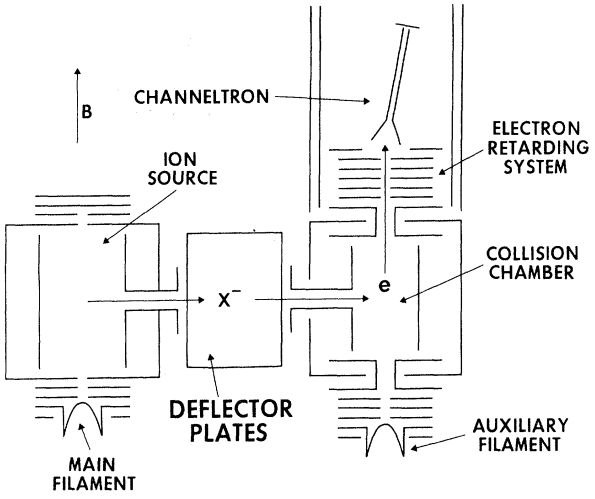

FIG. 1. Schematic diagram of the apparatus used for the measurement of associative detachment reactions.

ergy and has not included the energy analysis of the resulting electrons. The initial investigators observed negative-ion loss as a function of the reactant gas density. Fehsenfeld, Ferguson, and Schmeltekopf,[14] using a flowing afterglow, have measured many rate constants for associative detachment of ions with approximately thermal energy. Moruzzi and Phelps[15] have used a drift tube to measure rate constants for several associative detachment reactions at ion energies slightly above thermal. In these experiments, the final products of the reactions were not observed. In a subsequent experiment, Moruzzi, Ekin, and Phelps[16] did measure electrons from associative attachment. Indeed, Moruzzi *et al.* were able to vary the O^--ion energy up to 0.16 eV in the laboratory frame and observed that the detachment rate constants for two systems, $O^- + CO$ and $O^- + H_2$, were relatively constant over this energy range. Yet in all this work the ion energy could not be varied over a large range, and the final state of the products could not be determined because energy analysis was not available.

This paper reports an experiment in which an ion beam, with variable energy and relatively good energy resolution, impinges on a chamber filled with reactant gas. The detached electrons are energy analyzed using retarding potentials. Through the use of beam techniques, it is possible to extend the range of the ion energy while maintaining good energy resolution.

When the ion energy is large enough, other reactions, in addition to associative detachment, become possible. The most important is direct collisional detachment which is often difficult to separate from associative detachment.

Sections II and III of this paper describe the experimental apparatus and its operation. Section IV describes the method used for data accumulation. The data are presented and discussed in Secs. V–X, which describe the particular reactions: $O^- + CO$; $O^- + H_2$; and $O^- + O_2$.

II. APPARATUS

The experimental tube, shown schematically in Fig. 1, consists of a negative-ion source for producing ions by dissociative attachment, a set of deflector plates for steering the ions into the collision chamber, the collision chamber, and an electron retarding system. The tube is mounted in a stainless-steel envelope above a 6-in. oil diffusion pump and is isolated from the pump by a large liquid-nitrogen trap. The pumping speed is about 1000 l/sec. A background pressure of 5×10^{-9} Torr is obtained after baking the system at ~200 °C for 60 h. A magnetic field of about 100 G throughout the chamber is produced by two external coils.

The ion source produces negative ions from the dissociative attachment reaction $e + O_2 \rightarrow O^- + O$. The electron beam for this reaction is obtained from a thoria-coated iridium filament. The electron beam, usually 10 μA, passes through the ion-source chamber which is filled with oxygen gas to a pressure of about 10^{-2} Torr. The pressure outside the chamber is usually three orders of magnitude smaller.

The negative ions produced in the ion source are extracted through a channel (4 mm diam and 17 mm long) attached to a plate; the opposing plate is maintained at a small negative potential and is used as a pusher.

Ions produced by secondary reactions are prevented from leaving the ion source. The production of O_2^- by the charge-transfer reaction $O^- + O_2 \rightarrow O + O_2^-$ takes place in the ion source because the O^- produced by dissociative attachment reaction has sufficient energy. However, the O_2^- ion, whose initial energy is low, does not leave the ion chamber because its radius in the magnetic field is too small. Further, because we find that the negative-ion current leaving the ion source varies linearly with the pressure in the ion source, we are confident that secondary ions are absent in the beam.

The deflector plates following the ion source are used for collimating the beam before entrance into the collision chamber and for increasing the energy resolution of the beam. The region containing the deflector plates is highly pumped to avoid secondary collisions and to prevent gas from the ion source leaking into the collision chamber. The ion beam passes through a channel into a field-

free collision chamber and is finally collected on a collector electrode. The pressure of the target gas in the collision chamber (CO, H_2, or O_2) is about 10^{-2} Torr, and the pressure outside the chamber is about three orders of magnitude lower.

The electron retarding system (see Fig. 1) consists of an exit channel in the collision chamber, a guard plate with a 0.5-mm hole, and three retarding plates. Detached electrons, traveling along the magnetic field, pass through the exit electrode and the guard plate into the retarding region defined by 0.5-mm holes in the retarding plates. Two guard plates following the retarding region reduce the penetration from the high potential of the channeltron electron multiplier which serves as the collector for detached electrons. The whole retarding and counting section is contained in a double cylindrical shield; the outside shield is grounded while the inside shield is connected to the exit electrode of the collision chamber. The spiraltron electron multiplier is tilted slightly to offset the effect of the magnetic field; with 200 V applied to the front cone and 3600 V applied along the length of the multiplier, the gain is about 1000.

The electronics for handling the channeltron pulses consist of a floating preamplifier, an isolating pulse transformer, an amplifier, a discriminator, and a 24-bit counter. In practice, the preamplifier is operated in a current gain mode to minimize noise. The pulse width is degraded by the transformer and the amplifier, limiting the maximum count rate to 5×10^5 counts per sec. This maximum counting rate is more than sufficient to handle the maximum experimental counting rate which is about 10 counts per sec. The background noise is 0.1–0.3 counts per sec, comparable to the lowest signal studied. The discriminator is operated in a relatively insensitive region to eliminate errors due to drift in threshold level.

An auxiliary electron gun (see Fig. 1) consisting of an iridium filament and three plates for control and collimation is mounted opposite the retarding section. The electron beam from this gun passes through the collision chamber, and it is used to align and test the retarding system. It is inoperative when actual experiments are performed.

III. OPERATION

We employ two modes of operation to explore the associative detachment reactions. The first mode yields the cross section for total electron detachment, while the second mode gives electron energy distributions. Both modes can give information on the potential surfaces of the compound states.

A. Total Collection

The first mode involves collecting the current of detached electrons as a function of the ion energy. To change the ion energy, the potential of the collision chamber and the electron retarding system are swept, as a unit, with respect to the ion source and the deflector plates. This allows the ion beam to be accelerated or decelerated in passing from the deflector plates into the collision chamber.

The O^- beam intensity changes dramatically over the lower end of the energy range considered. At very low ion energy, the ion current drops to 10^{-14} A; at higher energy, the ion current reaches about 2×10^{-12} A. The fluctuations associated with the ion beam and its measurement are 3×10^{-15} A. Because of the change in beam intensity, the relative intensity at every energy must be used to normalize the electron counts collected for that ion energy. Systematic errors in the measurement of the beam intensity are estimated to be $\pm10\%$.

To gain confidence in the linearity of the energy scale of the ion beam, structure in the total cross section for electron detachment ($O^- + CO$) is remeasured for different beam conditions. Every condition of the deflector plates that preserves the same resolution also maintains the same separation of the observed structure.

At low ion energy, the background signal is significant and must be subtracted from the measured signal. Two kinds of background counts appear in this energy range. The first is noise, i.e., counts that are independent of the negative-ion beam. The second is electron detachment from O^- colliding with the small background of O_2 which effuses from the ion source. Since this background is energy dependent, the total background must be measured at every energy where total detachment is measured. The background is determined by varying the pressure of the target gas in the collision chamber and noting the pressure-independent signal at low pressures of the target gas. This background is then subtracted from the total signal.

B. Energy Distribution

The second mode of operation involves measuring the energy distribution of the detached electrons for a given O^- energy. This is accomplished by sweeping the potential of the three retarding plates with respect to the collision chamber. Differentiation of the resultant curve yields an electron energy distribution.

The measured electron energy distributions are distorted by the magnetic field. Because the detached electrons in the collision chamber scatter at all angles, most of the electrons entering the retarding region have velocity components perpendicular to the magnetic field. Therefore, the velocity along the field, the measured parameter, is not necessarily a measure of the total electron energy. Only electrons scattered at 90° with re-

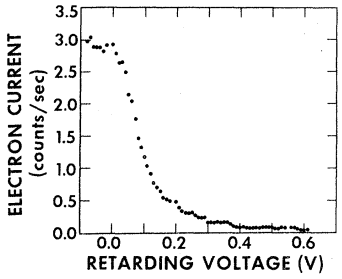

FIG. 2. Retarding curve for electrons produced in the associative detachment reaction of O^- with CO.

spect to the ion beam exhibit the real energy of the resultant electrons, because only those electrons have all their momentum directed along the field. But, because large angular anisotropy is not expected in this experiment,[17] the distributions should be peaked near the real energy of the electrons.

IV. DATA ACCUMULATION

The storage and accumulation of data is accomplished with a PDP/8 computer. The negative-ion current is measured using a vibrating-reed electrometer whose output is monitored by a nine-bit signed analog-to-digital converter which can transfer data to the computer. The channeltron pulses resulting from detached electrons are counted on a 24-bit counter which can also transfer data to the computer. Timing of the experiment is accomplished with a 1-msec clock on the interrupt bus of the computer. The clock maintains the synchronization between a staircase voltage which sweeps the potentials and the channel advance of the data block. Therefore, every channel corresponds to a given potential.

A. Total Collection

In the total collection mode, the data are averaged by long-term accumulation. The electron counts and the ion beam signal are stored in two concurrently running data blocks, and the runs are successively added. Normalization of the electron counts is accomplished by dividing the data block containing the electron counts by the data block containing the ion beam measurement, point by point.

Transients resulting from the steps in the staircase, as well as the flyback from the end of the staircase to the beginning, are relatively large. Therefore, a large time delay is used not only before the start of each sweep but also before the beginning of each data channel.

B. Energy Distribution

In the energy-distribution mode, the data are also averaged by long-term accumulation. Electron counts are stored in a data block whose successive channels correspond to an incremented retarding potential. Because each retarding potential corresponds to collection of electrons above a certain velocity, each channel of the data block contains, sequentially, electrons with a higher velocity cutoff. Figure 2 shows an example of an experimental retarding curve.

Differentiation of the retarding curves yields electron energy distributions. Because the count rate is so small, this cannot be done with lock-in techniques. Differentiating by hand and by computer fit has been tried, but a more sensitive and useful technique is actually employed. The retarding curves are differentiated by taking the difference between two points on the retarding curve separated by some small potential ΔV. The result is proportional to the experimental energy distribution when ΔV approaches zero. Values between 20 and 50 meV are used for ΔV depending on the count rate. Smaller values require abnormally long accumulation times, whereas larger values degrade the resolution of the differentiation. The potential ΔV is usually larger than the resolution of the electron retarding system.

For convenience as well as accuracy, two retarding curves are measured in this experiment. Equivalent channels in each data block are measured at potentials separated by ΔV, so that the subsequent subtraction of one from the other, point by point, yields an on-line differentiation of the retarding curves. Examples of the differentiation producing electron energy distributions can be seen in the data section, where the differentiation of each retarding curve, as well as the on-line differentiation, is used.

In the measurement of the electron energy distributions, a special form of random-walk averaging is used to eliminate the influences of spikes which may occur at random intervals. These spikes are impossible to average because of their infrequent occurrence. Therefore, their effect is large especially since a relatively small number of channels are used to accumulate the data. This form of data accumulation takes two steps. First, a representative retarding curve is taken which is free of spikes. Subsequently, each incoming measurement of the retarding curve is compared to the stored curve. The points of the stored retarding curve are incremented by unity, decremented by unity, or left unchanged as a result of the comparison. The incoming measurement is then discarded. Therefore, the effect of a spike is only an increase of unity in the stored point which is easily erased on a subsequent run. The noise inherent in this method of accumulation is proportional to the square root of the absolute value of the stored data, while the amplitude of the derivative depends on the potential ΔV.

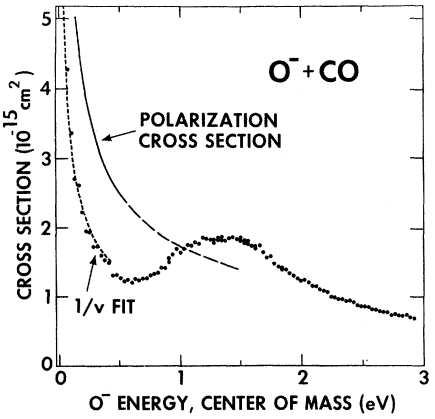

FIG. 3. Cross section for total electron detachment for the reaction of O^- with CO. The lower dashed line is the $1/v$ fit while the upper line is the polarization cross section. The closed circles are data points. The magnitude of the experimental cross section is calibrated using a thermal energy rate constant of 5.6×10^{-10} cm^3/sec with the uncertainty estimated to be ± 30%. The polarization cross section was calculated using a polarizability of 19.5×10^{-25} cm^3 for CO.

V. TOTAL DETACHMENT: $O^- + CO$

The cross section for electron detachment for the reaction of O^- with CO, as a function of O^- energy, is shown in Fig. 3. The O^- energy will henceforth be given in the center-of-mass system. It can be seen that, at very low O^- energy, the cross section falls sharply as the negative-ion energy is increased and exhibits a broad peak at moderate O^- energy. The solid line in Fig. 3 shows the polarization cross section σ_p, which varies as the inverse of the velocity,[18]

$$\sigma_p = 2\pi(\alpha e^2/2E)^{1/2},$$

where α is the average polarizability of the target, e is the ionic charge, and E is the energy in the center-of-mass system. Although the polarization cross section σ_p is the maximum possible collision cross section in the low-energy region, Herzenberg[13] has shown that the maximum cross section departs from the polarization cross section at an energy E_c, which depends on the internuclear separation R_D at which detachment begins. Thus the maximum cross section σ_D can be expressed as

$$\sigma_D = \sigma_p, \qquad E < E_c$$

$$\sigma_D = \pi R_D^2(1 + E_c/E), \qquad E > E_c .$$

The theoretical cross section in the high-energy region is always greater than the polarization cross section. This is reflected in the experimental data of Fig. 3 by the peak of the cross section rising above the polarization cross section at about 1 eV. Our calibration procedure relies on the absolute value of the associative detachment cross section at thermal energies, which is known to only ± 30%, as will be discussed below. Thus we cannot attach too much significance to the circumstance that the experimental data lie above the polarization section at about 1 eV.

The energy E_c can be estimated from the relation $E_c = \alpha e^2/2R_D^4$. Using a value of 2 Å for R_D, the critical energy is 0.9 eV. Since the value of E_c is so sensitive to the choice of R_D, this estimate is only approximate.

The potential-energy curves for the ground state of $CO_2 + e$ and the lowest states of CO_2^- are shown schematically in Fig. 4, as a function of the internuclear separation of the O atom from the static OC molecule. The model represented by these curves is both linear and diatomic; the axis of the OC molecule is always aligned with the approaching or the departing O^- ion.

The potential-energy curves may be used to explain the behavior of the experimental cross section. At very low ion energy (~ < 0.6 eV), the system does not have enough energy to reach the autoionization region along the repulsive CO_2^- ($^2\Sigma_g^+$) curve, i.e., the region of internuclear separation bounded by the crossing point of the CO_2^- ($^2\Sigma_g^+$) and the CO_2 ($^1\Sigma_g^+$) curves. Direct detachment ($O^- + CO \rightarrow O + CO + e$) is also not possible because it has a threshold of 1.465 eV. Therefore, the system can undergo electron detachment at low energy only via the attractive CO_2^- state, because only this path leads to the autoionization region. Using the statistical weights of the $^2\Pi_u$ and the $^2\Sigma_g^+$ states of CO_2^-, we find that 67% of all collisions are expected to follow the path of the $^2\Pi_u$ state. We show below that not all trajectories along the $^2\Pi_u$ state

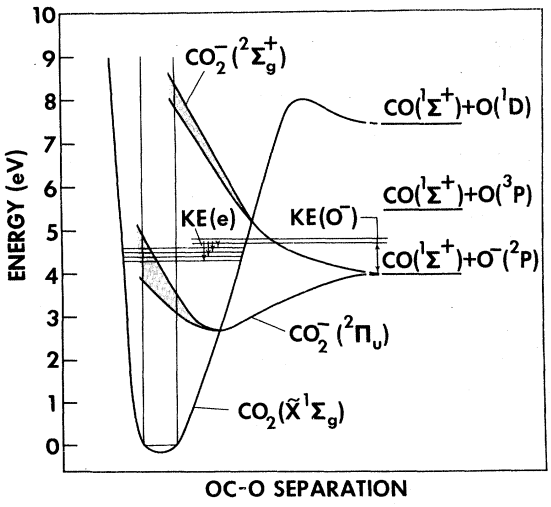

FIG. 4. Potential-energy curves of $CO_2 + e$ and CO_2^-. The bending angle is 180°.

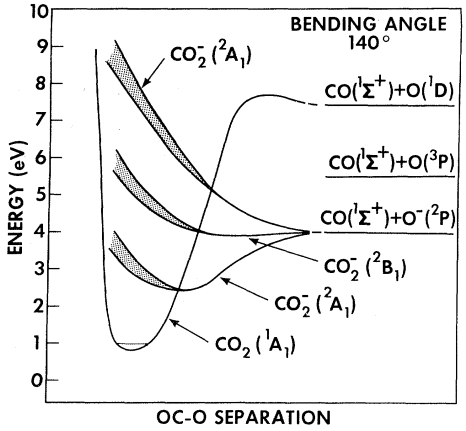

FIG. 5. Potential-energy curves of CO_2+e and CO_2^- states as derived from the calculations of Claydon *et al.* (Ref. 19).

lead to the autoionization region, and thus, we expect the cross section for associative detachment to be less than 67% of the polarization cross section. The experimental value from Fig. 3 is 55%.

The potentials for CO_2 and CO_2^- are actually multidimensional surfaces, functions of four internuclear variables. The appropriate surface has been calculated by Claydon, Segal, and Taylor.[19] Although they show only two-dimensional cuts of the surface, the potential energy of CO_2^- as a function of the bond angle for a given OC-O separation is instructive since the experiment measures a cross section averaged over many bond angles. Actually, because of the nature of orbiting collisions, it may be more appropriate to average over many angles of interaction, at least for low-energy collisions. Claydon *et al.*[19] show that, at an internuclear separation (OC-O) of 1.230 Å, the $^2\Pi_u$ state of CO_2^- removes its degeneracy upon bending and splits into two states $^2A_1$ and $^2B_1$. The $^2A_1$ state remains attractive for most angles, but the $^2B_1$ state becomes repulsive at some large angle. This result would be more relevant if data were available for larger internuclear separations; the internuclear separation of 1.230 Å is near the ground-state equilibrium point, well into the autoionization region.

The low-detachment cross section observed experimentally can now be understood as the inability of the system in the CO_2^- ($^2\Pi_u$) state to reach the autoionization region in all collisions. A schematic set of potential curves, derived from the results of Claydon *et al.*,[19] is shown in Fig. 5 for a bond angle of 140°. Here it is more obvious that, for low-energy ions, the system does not have enough energy to reach the autoionization region when following the repulsive $^2B_1$ state. If we assume that the $^2B_1$ does not contribute at all to associative detachment, then the cross section for associative detachment would be 33% of σ_p, i.e., somewhat smaller than the observed value of 55%. Therefore, we conclude that both the $^2B_1$ and $^2A_1$ states contribute to the associative detachment cross section at low ion energy. This conclusion is based on the calibration of the absolute cross-section scale, which is discussed below.

At higher negative-ion energy, the repulsive portions of the potential curves are expected to contribute to detachment because the system has enough energy to reach the autoionization region. When the ion energy reaches approximately 1.5 eV, where all the CO_2^- states (including the $^2\Sigma_g^+$ state) contribute to associative detachment, the total detachment cross section approaches the theoretical maximum. This supports what has heretofore been an implicit assumption; almost all collisions which can detach, will do so. This is equivalent to saying that the average lifetime $\bar{\tau}$ of the resultant CO_2^- state is so short that very little O^- can escape, which puts an upper bound of one vibrational period on the average lifetime. Therefore, the average width $\bar{\Gamma}=\hbar/\bar{\tau}$ of the CO_2^- states must be large.

A peculiar region indigenous to CO_2 exists above an ion energy of 1.465 eV. Although the lowest separated states of CO ($^1\Sigma^+$) and O (^3P) lie at only 5.45 eV above the ground state of CO_2, the ground state itself is correlated to the higher-lying asymptote of the separated CO ($^1\Sigma^+$) and O (^1D) at 7.41 eV. Thus, direct detachment can occur via one of the states correlated with the lower asymptote while associative detachment can still proceed to the ground state of CO_2, both of which can yield low-energy electrons. These reactions are not easily separated.

In this high-energy region, the experimental cross section falls faster than expected. Although this anomaly is not well understood, we can speculate that a reaction volume exists in which detachment will not occur, i.e., a region in which the potentials of the CO_2 ground state and the higher repulsive potentials (leading to direct detachment) are above the CO_2^- potential. If such a volume did exist, fast collisions (without appreciable orbiting) would lead to an increasing number of collisions within the bounds of the unfavorable volume. This leads to a limiting cross section, at high energy, which would be below the geometrical limit proposed by Herzenberg.[13]

The low-energy region is approximated by a $1/v$ functional form while using a χ^2 test for goodness of fit.[20] The zero of negative-ion energy is determined from the low-energy fit by minimizing χ^2 as a function of the point of zero energy. On five sets of data taken at low energy, the zero shifted by no more than 20 meV. The point of

zero energy calculated from the known energy of the ions is always within 50 meV of the fitted zero. χ^2 is low enough to indicate a confidence of greater than 99.999% in the goodness of fit and is sensitive enough to locate the zero energy within ± 10 meV.

The magnitude of the cross section is calibrated by using the value of the fitted curve at thermal energy. Fehsenfeld, Ferguson, and Schmeltekopf[14] have reported a value of $\sim 5\times10^{-10}$ cm^3/sec, later corrected to 5.6×10^{-10} cm^3/sec and, most recently, to 4.4×10^{-10} cm^3/sec for the detachment rate of the reaction of O^- with CO at thermal energy.[21] Moruzzi, Ekin, and Phelps[16] have reported a value of $\sim 6.3\times10^{-10}$ cm^3/sec with ion energies just above thermal energy. We adopt the value of 5.6×10^{-10} cm^3/sec, which yields the cross section for thermal energy ions of 7.14×10^{-15} cm^2. There is an uncertainty of approximately ± 30% in this calibration.

VI. ENERGY DISTRIBUTIONS: O^- + CO

Three electron energy distributions taken for various O^- energies ranging from 0.09 to 1.55 eV are shown in Fig. 6. The differentiation width is 20 meV for all distributions. The error bars represent one standard devation calculated from repeated measurements. It can be seen that all the distributions contain only low-energy electrons; this indicates that the CO_2 molecule is left in a highly excited state, with more than 3 eV of energy retained in vibrational and rotational excitation. By estimating the maximum angular momentum in the collision, a limit of 50 meV can be placed on the energy in rotational modes. Therefore, almost all the excess energy must be in vibrational excitation. The vibrational spacing of the bending mode at and above 3 eV is approximately 67 meV, calculated by using only the first anharmonic coefficient. For the asymmetric and the symmetric stretch modes, the spacings are approximately 248 and 165 meV, respectively.

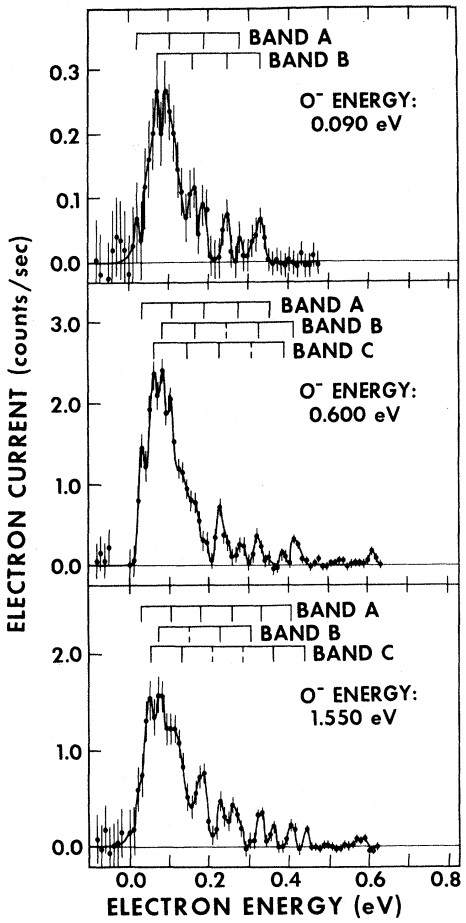

FIG. 6. Electron energy distributions for the reaction of O^- with CO for O^- energies of 0.09, 0.60, and 1.55 eV.

The electron energy distribution at an O^- energy of 0.09 eV is the least complex. Two progressions of peaks, each with a spacing about 80 meV, are visible and are shown in Fig. 6 by the bars above the distribution. The spacing between bands is 56 meV. The first member of each band corresponds to a CO_2 molecule with the highest excitation possible at that ion energy. Each succeeding member of a band corresponds to a CO_2 molecule, with one less quantum of energy in the bending mode. We conclude that the resultant CO_2 is preferentially excited in the bending mode for the associative detachment reaction of O^- with CO. This is not to say that other modes are not excited at the same time, but only to point out that large excitation of the other modes would mean a much higher density of states than is observed.

Each band is probably due to a single electronic CO_2^- state. At an O^- energy of 0.09 eV, only the two lowest CO_2^- states are accessible, the $^2B_1$ and $^2A_1$ states resulting from the linear $^2\Pi_u$ state. The separation of the bands can be attributed to different crossing points into the autoionization region and, therefore, a different combination of vibrational modes. As an example, the difference between one quantum of asymmetric stretch and three quanta of bending is about 50 meV.

As the O^- energy is increased, the preceding argument would lead us to expect a third band due to the upper repulsive $^2A_1$ state, connected with the linear $^2\Sigma_g^+$ state. This band is observed (band C, Fig. 6), starting between 0.3 and 0.6 eV (O^- energy) with the same bending-mode structure, and it is spaced 35 meV from band A.

As the O^- energy increases, the spacing of each progression changes from approximately 80 meV at an O^- energy of 0.09 eV to 73 meV at an O^- energy of 1.55 eV. This change is due to the anharmonicity of the bending mode and indicates that slightly less than half of the total energy is in the

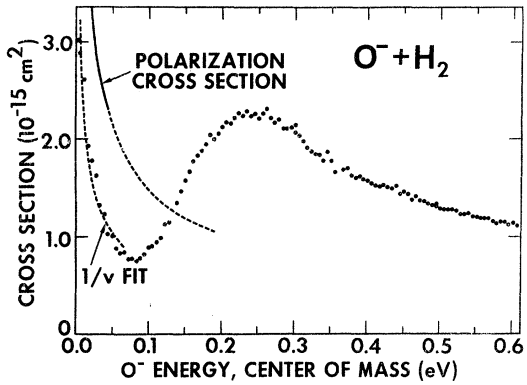

FIG. 7. Cross section for total electron detachment for the reaction of O^- with H_2. The lower dashed line is the $1/v$ fit while the upper line is the polarization cross section. The closed circles are data points. The magnitude of the experimental cross section is calibrated using a thermal energy rate constant of 7.5×10^{-10} cm^3/sec, which is known to ± 30%. The polarization cross section is calculated using a polarizability of 7.5×10^{-25} cm^3 for H_2.

bending mode.

An estimate of the width, and therefore the lifetime, can be made from these bands. The energy distributions extend over a range of about 600 meV. Although some of this spread is due to the initial velocity of the ion, most of the variation in final vibrational levels is probably due to the autoionization width. Therefore, we estimate the upper limit of the autoionization width near the crossing point of the potential-energy curves to be 0.6 eV and the corresponding lower limit of the lifetime is 1.1×10^{-15} sec. This should be compared to the approximate upper bound of the lifetime, one vibrational period of $\sim10^{-14}$ sec.

VII. TOTAL DETACHMENT: $O^- + H_2$

The cross section for electron detachment for the reaction of O^- with H_2, as a function of O^- energy, is shown in Fig. 7. At very low O^- energy, the cross section falls sharply as the negative-ion energy is increased and then exhibits a broad peak before falling again at higher energy. In contrast to the cross section for the associative detachment reaction of O^- with CO, which exhibits the same shape, the peak occurs at much lower O^- energy (~0.2 eV). The solid line in Fig. 7 shows the polarization cross section σ_p. It can be seen that the experimental cross section surpasses this cross section at low ion energy. Using 2 Å for the detachment radius, the maximum energy at which the initial departure from the polarization cross section should occur is 0.36 eV. Since the departure occurs at lower energies, we postulate that the detachment radius is larger than 2 Å, probably of the order of 3 Å.

The potential-energy curves for the ground singlet state of H_2O+e, the first triplet state of H_2O+e, and the lowest H_2O^- states are shown in Fig. 8, as a function of the internuclear separation of the O atom from the static H_2. These potentials and the other results discussed below, follow the calculations of Claydon, Segal, and Taylor[22] and are schematic at best. The ground-state H_2O ($^1A_1$) is bent, with an equilibrium bond angle of 105.2°, while the potential of the $^3B_1$ state seems to be very shallow as a function of bond angle with a possible minimum at 115°. At a bond angle of 180°, the $^3B_1$ state is degenerate with a $^3A_1$ state which has a potential minimum at 180° and is a very steep function of bond angle. These two triplet states have the lowest minima (~4.8 eV) with respect to the ground state that can be reached along the reaction coordinate. The first excited singlet state H_2O ($^1B_1$) has a potential minimum at ~5.8 eV and is not shown in Fig. 8, since it is above the range of this experiment.

Three H_2O^- states are shown in Fig. 8, all correlated with the separated O^- (^2P) and H_2 ($X^1\Sigma_g^+$) states. The lowest $^2A_1$ state is attractive with a minimum below 5 eV and an equilibrium bond angle of 136°. The $^2B_2$ and $^2B_1$ states are expected to be repulsive although the $^2B_2$ state may be shal-

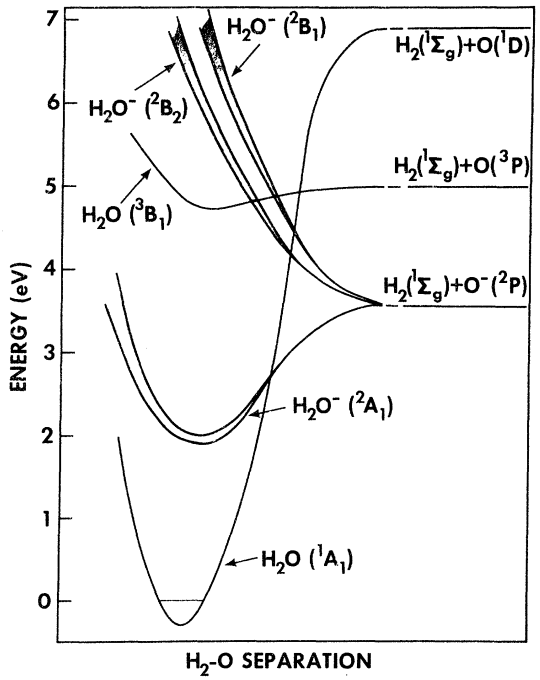

FIG. 8. Potential-energy curves of ground-state H_2O+e, the excited triplet state of H_2O^*+e, and the H_2O^- states as derived from the calculations of Claydon *et al.* (Ref. 22). The bending angle is 104°.

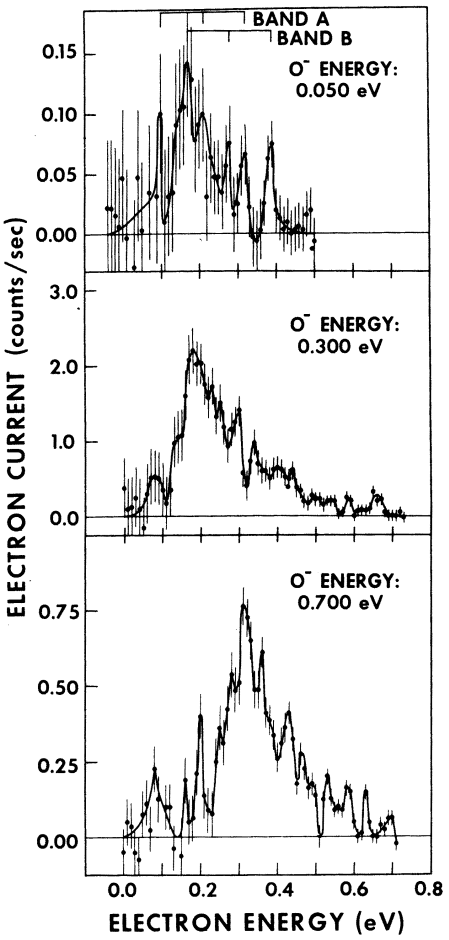

FIG. 9. Electron energy distributions for the reaction of O^- with H_2, for O^- energies of 0.05, 0.30, and 0.70 eV.

low or even attractive for some bond angles. The crossing points of these curves with the ground state of H_2O seem to occur below 5 eV.

These potential curves may be used to explain the behavior of the detachment cross section. At very low ion energy, the experimental cross section is ~48% of the polarization cross section. Since the low H_2O^- ($^2A_1$) state could contribute only 33%, at most, we conclude that some portions of the potential of the $^2B_2$ state must be attractive. Furthermore, the bond angle at which the potential is attractive is probably relatively small since, for this reaction where the oxygen must be inserted between the hydrogen atoms, the reaction coordinate is initially at some small angle.

The repulsive H_2O^- state would be expected to contribute to associative detachment as the ion energy becomes higher than the respective crossing points with the ground state of H_2O, i.e., as the system reaches the autoionization regions along these curves. The peak in the detachment cross section corresponding to initiation of associative detachment via the repulsive H_2O^- states occurs at relatively low ion energy (~0.27 eV). No other structure is noted in the detachment cross section for ion energies up to 1.7 eV, which corresponds to ~15 eV in the lab system. Therefore, the repulsive H_2O^- states must be relatively shallow along the path of the negative ion even though they appear at much higher energy in the Franck–Condon region, as determined from dissociative attachment. Furthermore, since the detachment cross section is so large in this region, the average lifetime of the H_2O^- state must be very short, probably bounded by one vibrational period.

For ion energies higher than 0.3 eV, the experimental cross section decreases faster than expected. This decrease is not understood, although we can again speculate, as for the (O^-, CO) system, that associative detachment can only occur in a limited volume and that the nature of the faster collisions precludes entry into this volume during some collisions. This leads to a limiting geometrical cross section which is below the expected cross section.[13]

The low-energy region of the detachment cross section is fitted to a $1/v$ functional form while using a χ^2 test for goodness of fit[20] (see Fig. 7). The zero of negative-ion energy is determined from the $1/v$ fit by minimizing χ^2 as a function of the point of zero energy. This zero had not shifted from the zero previously determined for the (O^-, CO) system. Repeated measurements shifted by no more than 5 meV. χ^2 is always small enough to indicate a confidence of greater than 99.999% in the goodness of fit.

The magnitude of the cross section is calibrated by using the value of the fitted curve at thermal energy. Fehsenfeld, Ferguson, and Schmeltekopf[14] have reported a value of 1.5×10^{-9} cm^3/sec, later corrected to 8.6×10^{-10} cm^3/sec, and most recently, 6×10^{-10} cm^3/sec for the detachment rate of the reaction of O^- with H_2 at thermal energy.[21] Moruzzi, Ekin, and Phelps[16] have reported a value of 7.5×10^{-10} cm^3/sec with ion energies just above thermal energy. We adopt the value of 7.5×10^{-10} cm^3/sec, and thus, the cross section for thermal energy ions is $\sim4\times10^{-15}$ cm^2. The uncertainty in this calibration is estimated to be ±30%.

VIII. ENERGY DISTRIBUTIONS: $O^- + H_2$

Three electron energy distributions, for O^- energies varying from 0.05 to 0.70 eV, are shown in Fig. 9. The differentiation width is 20 meV in all distributions. The error bars reflect the scatter of repeated measurements and, for unknown reasons, are usually larger than the errors in the reaction $O^- + CO \rightarrow CO_2 + e$. It can be seen that the distributions are peaked at low electron energy

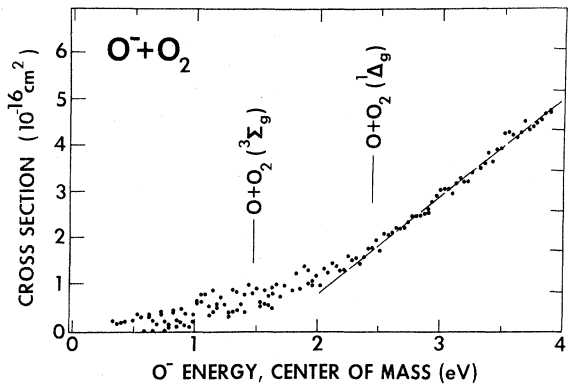

FIG. 10. Cross section for total electron detachment in the reaction of O^- with O_2. The closed circles are data points. The dashed line is a linear least-squares fit to the data points.

corresponding to a highly excited H_2O molecule. Although the main peak of the distribution shifts as a function of the ion energy, over 3 eV must be retained in the molecule in every case. Claydon *et al.*[22] have shown that the triplet states of H_2O lie just above the energy range used in this experiment and thus, are not accessible. Therefore, the excess energy must be in vibrational and rotational modes of the ground electronic state of H_2O. By estimating the maximum angular momentum in the collision, the maximum energy in rotational modes is 0.05 eV. Therefore, most of the excess energy is in vibrational excitation of ground-state H_2O.

The least-complex electron energy distribution is at the lowest ion energy (0.05 eV). Two progressions of peaks are observed, each with a variable spacing near 105 meV. The bands are spaced 40 meV apart. Although the second vibrational mode (i.e., bending mode) of ground-state H_2O has a spacing of 200 meV at the bottom of the potential, the anharmonicity of the mode is large. At 3-eV energy, the bending mode has a spacing of 105 meV. The other vibrational modes of H_2O, whose spacings are 458 and 471 meV, could not account for the observed structure. Therefore, we conclude that the bending mode is preferentially excited during the associative detachment reaction of O^- with H_2, even though some excitation of the other modes is probable.

The spacing between the bands could be attributed to a different partitioning of the energy into the vibrational modes caused by autoionization from different points on the potential surfaces. At this ion energy, only the $^2A_1$ and $^2B_2$ states of H_2O^- are expected to play a role in associative detachment as discussed in Sec. VII. Thus, each band could be due to a single H_2O^- state whose potential causes different combinations of vibrational modes to be excited. The observation that the spacing between bands changes as a function of electron energy, as well as ion energy, does not affect the argument because the anharmonicity of the vibrational modes is so large.

The spacing of each progression changes as a function of the ion energy from near 105 meV for 0.05-eV O^- energy to ~75 meV for 0.7-eV O^- energy. Since the vibrational spacing of the bending mode becomes ~75 meV near 3.4 eV, the change is assumed to be caused by an increase in the bending-mode excitation from 3 to ~3.4 eV and shows that the bending mode contains approximately 75% of the excess energy at all ion energies. This observation also supports our conclusion that the bending mode is preferentially excited.

At higher ion energy, the main peak of the electron energy distributions shifts to higher energy, indicating that the lifetime for the H_2O^- states is probably longer than for CO_2^- states. The electron energy distributions become rather complex and difficult to interpret.

IX. TOTAL DETACHMENT: $O^- + O_2$

The cross section for electron detachment for the reaction of O^- with O_2, as a function of O^- energy, is shown in Fig. 10. The cross section is very small at low energy, rising linearly at higher energy. The calibration of the magnitude of the experimental cross section is made by comparison with the cross section for the reaction of O^- with CO, and the data taken at higher energy match, within 30%, the values of the detachment reactions of O^- with O_2, obtained by Bailey and Mahadevan.[23]

The potential-energy curves for the lowest states of $O_3 + e$ and a state of O_3^- are shown in Fig. 11 as a function of the internuclear separation of the O atom from the static O_2 molecule. Very little is known about the actual potential curves of O_3 and O_3^-, so that these curves are merely schematic and show only the main features.[24] The drawing represents a diatomic model.

Although the shapes of the potential curves are hypothetical, they may be used to explain the behavior of the detachment cross section. At very low ion energy, the system does not have enough energy to detach, because the dissociation energy (O-O_2) is 1.07 eV, whereas the electron affinity of O is 1.465 eV. Therefore, in this system, associative detachment has a theoretical threshold of at least 0.39 eV.

The cross section for associative detachment σ_{AD}, just above the threshold can be estimated from the cross section for the dissociative attachment reaction $e + O_3 \rightarrow O^- + O_2$, by detailed balance using the relation[25]

$$\sigma_{AD} = \sigma_{DA}(k_{AD}^2/k_{DA}^2) ,$$

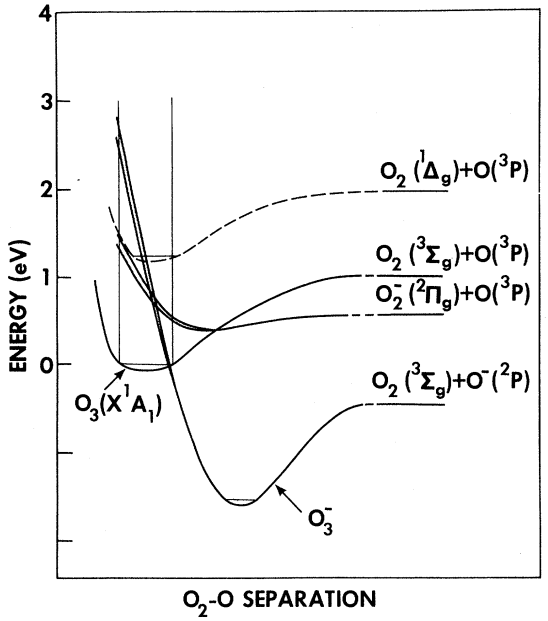

FIG. 11. Schematic diagram of the potential-energy curves for the ground state of O_3+e and the O_3^- states. The dashed curve represents the first excited O_3 state.

where σ_{DA} is the dissociative attachment cross section, $\lambda\!\!\!^{-}_{AD}$ is the channel wavelength for the (O^-, O_2) system, and $\lambda\!\!\!^{-}_{DA}$ is the channel wavelength for the (e, O_3) system. Here λ is the deBroglie wavelength, $\lambda\!\!\!^{-}=\hbar/(\mu v)$, where h is Planck's constant, μ is the reduced mass, and v is the relative velocity. Unlike the previous systems, the first open channel for associative detachment is the ground vibrational state which is also the state from which dissociative attachment is measured. Using the value of the dissociative attachment cross section (1.9×10^{-17} cm^2) for the peak at an electron energy of 1.25 eV, recently reported by Chantry,[26] the cross section for associative detachment is $\sim2\times10^{-21}$ cm^2 for O_3 in the ground vibrational state and an ion energy ~1.6 eV. The experimental cross section at an ion energy of 1.6 eV is $\sim10^{-16}$ cm^2. Thus, detailed balancing underestimates the associative detachment cross section, which implies that the dissociative attachment cross section for higher-lying vibrational states is larger than that from the ground vibrational state.

The cross section calculated by detailed balance is an upper limit for the associative detachment reaction at threshold. Since 3×10^{-17} cm^2, is the smallest cross section measurable in the present experiment, the actual threshold cannot be seen in Fig. 10.

At high ion energies, direct detachment becomes possible; the first threshold for the direct detachment process

$$O^- + O_2 \rightarrow O + O_2\,(^3\Sigma_g^-) + e$$

is 1.465 eV. The experimental cross section rises linearly between 2 and 4 eV, and the extrapolated intercept occurs at 1.67 eV. Because the extrapolated intercept is not 1.465 eV, we conclude that at least one other process is competing at higher ion energy. Possible detachment reactions are associative detachment to the electronically excited states of O_3, direct detachment via a repulsive state, and the direct-detachment reaction

$$O^- + O_2 \rightarrow O_2\,(^1\Delta_g) + O + e\ .$$

X. ENERGY DISTRIBUTION: $O^- + O_2$

An electron energy distribution, measured at an O^- energy of 2.58 eV for the reaction of O^- with O_2, is shown in Fig. 12. Three main peaks are visible at 450, 286, and 179 meV. The differentiation width is 50 meV. The error bars represent approximately the square root of the total number of counts at each point on the retarding curves and are indicative of the actual scatter of repeated measurements. The peaks are not understood although they could be explained by either repulsive states leading to $O+O_2$ or associative detachment to an excited state of O_3.

XI. CONCLUSION

The cross sections for total electron detachment for the reactions of O^- with CO and H_2 have similar shapes. Near zero ion energy, they both follow the form of the polarization cross section. The process in this region is associative detachment via the attractive potential-energy curves of the compound states. For intermediate ion energies, both cross sections exhibit a broad peak at 0.3 eV for H_2 and 1.5 eV for CO, which results from associative detachment via the repulsive potential-energy curves of the compound states. For higher ion energies >~5 eV both cross sections approach a finite limit as suggested by Herzenberg.[13]

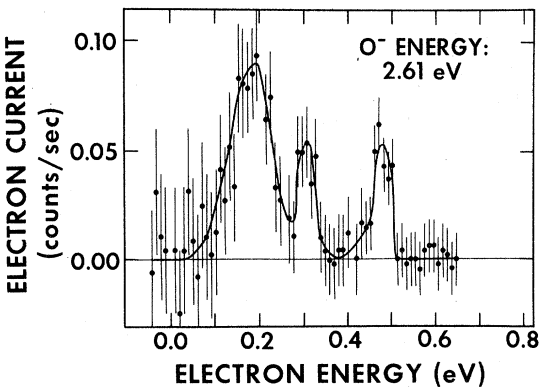

FIG. 12. Electron energy distribution for the reaction of O^- with O_2 at an ion energy of 2.6 eV.

Claydon *et al.*[19,22] have shown that the potential-energy curves change as a function of the bending angle and that, as a result, associative detachment may occur only along some paths of the potential surfaces while other paths require more energy.[14] These considerations are confirmed in the present experiment by noting that the limit, which the cross sections approach at high energy, is lower than expected.

The electron energy distributions for the reactions of O^- with CO and H_2 exhibit low-energy peaks corresponding to high vibrational and rotational excitation of the resultant molecule. Progressions observed in these distributions have spacings corresponding to the bending mode of the resultant triatomic molecule. In the reaction $O^- + CO \rightarrow CO_2 + e$, the observed bands indicate that the vibrational excitation of the bending mode of CO_2 accounts for nearly 50% of the excess energy, except at very low ion energy where the proportion is less. In the reaction $O^- + H_2 \rightarrow H_2O + e$, the observed bands indicate that the vibrational excitation of the bending mode of H_2O accounts for nearly 75% of the excess energy.

The interpretation of the structure in the electron energy distribution ignores the possibility that some contribution to the structure may result from the splitting of the ground state of O^-. The ground state of O^-, having a ^2P configuration can have $J = \frac{1}{2}$ and $\frac{3}{2}$ states. The energy difference between these two states is not firmly established,[27-29] nor is the relative yield of $^2P_{3/2}$ and $^2P_{1/2}$ ions in dissociative attachment of O_2. Thus, we are not able to determine what effect these two states have on our electron energy distributions.

The cross section for total electron detachment for the reaction of O^- with O_2 exhibits a threshold near 0.7 eV and rises linearly at higher energy. The low-energy region ($\sim < 1.465$ eV) of the cross section is believed to be due to the associative detachment reaction $O^- + O_2 \rightarrow O_3 + e$. Above that energy, the major process is believed to be direct detachment. Since the extrapolated threshold of the linear portion of the cross section is above 1.465 eV, we believe that processes with higher thresholds are involved, such as associative detachment to an excited state of ozone or direct detachment to repulsive $O + O_2$ states. This suggestion is supported by the electron energy distribution taken at an O^- energy of 2.5 eV.

ACKNOWLEDGMENTS

We wish to thank A. Herzenberg for many helpful discussions on the theory of associative detachment. We also wish to acknowledge the useful comments and criticisms of P. D. Burrow, M. J. W. Boness, D. Spence, and A. V. Phelps, as well as the technical assistance of J. H. Kearney.

APPENDIX: χ^2 TEST

A parametrized $1/v$ curve is fit to the curves for total detachment at low ion energy for the reactions of O^- with CO and H_2. The theoretical curve, in discrete form, is given by the relation

$$p_i = (a/n)(E_i - E_0)^{-1/2},$$

where a and E_0 are parameters which allow the magnitude to be scaled and the zero to be shifted. E_i is the measured ion energy and n is a normalization constant calculated by requiring that

$$\sum_i^r p_i = 1 .$$

Therefore, n is given by the relation

$$n = \sum_i^r a(E_i - E_0)^{-1/2},$$

where r is the total number of measured points.

A modified least-squares fit is performed by minimizing the parameter χ^2 given by the relation[20]

$$\chi^2 = \sum_i^r (\nu_i - np_i)^2/np_i ,$$

where ν_i is the measured value of the curve at the point E_i. The parameters a and E_0 are determined from this least-squares fit.

When χ^2 is minimized with respect to the parameter a, we find that

$$a = \left(\sum_i^r \nu_i^2 (E_i - E_0)^{1/2} \Big/ \sum_i^r (E_i - E_0)^{-1/2} \right)^{1/2},$$

which is independent of n. Although χ^2 could be minimized with respect to the parameter E_0 yielding another equation in a and E_0, the solution of the two equations is cumbersome. A computer solution is actually used and is accomplished by varying E_0 and by calculating χ^2 and the relative change in χ^2. In this way χ^2 is minimized with respect to the parameter E_0, and some measure of the sensitivity can also be estimated. By using the points at which χ^2 doubles as a criterion of the sensitivity, E_0 is determined within ± 10 meV. Within this range, the confidence in the goodness of fit remains greater than 99%.

---

†Work supported by the Defense Atomic Support Agency through Army Research Office, Durham and by the National Science Foundation.

*Present address: Joint Institute for Laboratory Astrophysics, University of Colorado, Boulder, Colo. 80302.

[1]H. S. Massey, *Negative Ions* (Cambridge U. P., Cambridge,

England, 1950).

[2]F. C. Fehsenfeld, A. L. Schmeltekopf, H. I. Schiff, and E. E. Ferguson, Planet. Space Sci. **15,** 373 (1967).

[3]A. Dalgarno, Ann. Geophys. **17,** 16 (1961).

[4]B. E. J. Pagel, Mon. Not. R. Astron. Soc. Geophys. Suppl. **119,** 609 (1959). This paper contains a communication from A. Dalgarno.

[5]A. L. Schmeltekopf, F. C. Fehsenfeld, and E. E. Ferguson, Astrophys. J. Lett. **148,** L155 (1967).

[6]D. R. Bates and H. S. W. Massey, Philos. Mag. **45,** 111 (1954).

[7]J. C. Browne and A. Dalgarno, J. Phys. B **2,** 885 (1969).

[8]J. N. Bardsley, A. Herzenberg, and F. Mandl, Proc. Phys. Soc. Lond. **89,** 305 (1966); Proc. Phys. Soc. Lond. **89,** 321 (1966).

[9]J. C. Y. Chen and J. L. Peacher, Phys. Rev. **167,** 30 (1968); Phys. Rev. **168,** 56 (1968).

[10]For the theory of complex potentials in atomic collisions, leading to associative detachment, see J. Mizuno and J. C. Y. Chen, Phys. Rev. A **4,** 1500 (1971).

[11]D. Rapp, T. E. Sharp, and D. D. Briglia, Phys. Rev. Lett. **14,** 533 (1965).

[12]G. J. Schulz and R. K. Asundi, Phys. Rev. **158,** 25 (1967).

[13]A. Herzenberg, Phys. Rev. **160,** 80 (1967).

[14]F. C. Fehsenfeld, E. E. Ferguson, and A. L. Schmeltekopf, J. Chem. Phys. **45,** 1844 (1966); for more results and discussions see also E. E. Ferguson, F. C. Fehsenfeld, and A. L. Schmeltekopf, J. Chem. Phys. **47,** 3085 (1967); F. C. Fehsenfeld and E. E. Ferguson, J. Chem. Phys. **51,** 3512 (1969); D. B. Dunkin, F. C. Fehsenfeld, and E. E. Ferguson, J. Chem. Phys. **53,** 987 (1970); F. C. Fehsenfeld, D. L. Albritton, J. A. Burt, and H. I. Schiff, Can. J. Chem. **47,** 1793 (1969); E. E. Ferguson, F. C. Fehsenfeld, and A. L. Schmeltekopf, Adv. Chem. Ser. **80,** 83 (1969); F. C. Fehsenfeld and E. E. Ferguson, J. Chem. Phys. **53,** 2614 (1970).

[15]J. L. Moruzzi and A. V. Phelps, J. Chem. Phys. **45,** 4617 (1966).

[16]J. L. Moruzzi, and J. W. Ekin, Jr., and A. V. Phelps, J. Chem. Phys. **48,** 3070 (1968).

[17]Angular distribution calculations of Ref. 9 are referenced to the internuclear axis of the diatomic target and the direction of the incident ion beam. However, when the internuclear axis is averaged over many directions, the angular distribution of the electrons becomes isotropic.

[18]E. W. McDaniel, *Collision Phenomena In Ionized Gases* (Wiley, New York, 1964), p. 72.

[19]C. R. Claydon, G. A. Segal, and H. S. Taylor, J. Chem. Phys. **52,** 3387 (1970).

[20]A discussion of χ^2 tests can be found in H. Cramer, *Mathematical Methods of Statistics* (Princeton U. P., Princeton, N. J., 1966), p. 416.

[21]A table of the reaction rates for associative detachment is given by E. E. Ferguson [in *Advances in Electronics and Electron Physics,* edited by L. Marton (Academic, New York, 1968), Vol. 24, p. 1], where values are reported for the reaction of O^- with CO (5.6×10^{-10} cm^3/sec) and for the reaction of O^- with H_2 (8.6×10^{-10} cm^3/sec). A more recent review is contained in E. E. Ferguson, Acc. Chem. Res. **3,** 402 (1970); the values of the reaction rates are 4.4×10^{-10} cm^3/sec for the reaction of O^- with CO and 6.0×10^{-10} cm^3/sec for the reaction of O^- with H_2.

[22]C. R. Claydon, G. A. Segal, and H. S. Taylor, J. Chem. Phys. **54,** 3799 (1971); calculations of the H_2O^- ($^2B_1$) state done by A. W. Weiss and M. Krauss [J. Chem. Phys. **52,** 4363 (1970)] for a single point on the potential surface of H_2O^-, suggest that the $^2B_1$ state is lower than shown in Fig. 9.

[23]T. L. Bailey and P. Mahadevan, J. Chem. Phys. **52,** 179 (1970); other data have been reported by A. E. Roche and C. C. Goodyear [J. Phys. B **2,** 191 (1969)] and by L. Frommhold [Fortschr. Phys. **12,** 597 (1964)].

[24]Calculations by W. M. Wun (unpublished) suggest that the internuclear separation of the ground state of O_3^- is approximately the same as the internuclear separation for O_3. If this is so, then a repulsive O_3^- state might be needed to account for the large charge transfer reaction, $O^- + O_2 \rightarrow O_2^- + O$.

[25]J. M. Blatt and V. F. Weisskopf, *Theoretical Nuclear Physics* (Wiley, New York, 1966), p. 337.

[26]P. J. Chantry, Twenty-fourth Annual Gaseous Electronics Conference, Gainesville, Fla., 1971 (unpublished).

[27]L. M. Branscomb, D. S. Burch, S. J. Smith, and S. Geltman, [Phys. Rev. **111,** 504 (1958)] give a value of 28 meV for the $^2P_{(3/2)} - {}^2P_{(1/2)}$ splitting of O^-. The value is derived from an isoelectronic extrapolation.

[28]R. S. Berry, J. C. Mackie, R. L. Taylor, and R. Lynch [J. Chem. Phys. **43,** 3067 (1965)] give a value of 35 meV based on a measurement of radiative capture.

[29]C. Lineberger and H. Hotop give a value of 22 meV based on an isoelectronic extrapolation of the ratio of the splitting of the ion to the atom (private communication).